Contents lists available at ScienceDirect

Journal of Alloys and Compounds

Thermoelectric properties of Pb-doped bismuth telluride thin films deposited by magnetron sputtering

Yang Zhou, Liangliang Li *, Qing Tan, Jing-Feng Li

State Key Laboratory of New Ceramics and Fine Processing, School of Materials Science and Engineering, Tsinghua University, Beijing 100084, People's Republic of China

A B S T R A C T

Nanocrystalline n-type bismuth telluride (Bi_2Te_3) thin films doped with lead (Pb) were deposited by radiofrequency magnetron sputtering. The effects of Pb doping on the carrier concentration and the thermoelectric properties of the Bi_2Te_3 thin film were investigated. Optimization of the carrier concentration significantly increased the Seebeck coefficient of the Bi_2Te_3 film and reduced the carrier thermal conductivity. These phenomena contributed to the enhancement of the thermoelectric properties of the Bi_2Te_3 film. Power factors of 2.50 and 2.15 mW K^{-2} m^{-1} were achieved at 473 K for the as-deposited and annealed Bi_2Te_3 films with Pb doping concentration of 0.38 at.%, respectively. The experimental data demonstrate that Pb doping can effectively control the carrier concentration of the n-type Bi_2Te_3 film. The Pb-doped Bi_2Te_3 film is a promising material for thermoelectric microdevices.

© 2013 Elsevier B.V. All rights reserved.

1. Introduction

Thermoelectric materials have elicited considerable interest because of their ability to convert heat into electricity directly or vice versa [1,2]. Among the various thermoelectric materials, bismuth telluride (Bi_2Te_3)-based compounds are the most technologically useful materials for near-room temperature applications because of their relatively high thermoelectric efficiency [3–6]. The efficiency of thermoelectric materials is related to their figure of merit, which is defined as $ZT = S^2\sigma T/k$, where S is the Seebeck coefficient, σ is the electrical conductivity, T is the absolute temperature, and k is the thermal conductivity (including the carrier thermal conductivity k_c and the lattice thermal conductivity k_l). $S^2\sigma$ is defined as the power factor.

Thermoelectric microdevices, such as power generators [7,8] and cooling devices [9,10], have been intensively investigated because of their potential application in portable devices, power electronics, wireless sensor networks, and other fields. For microdevices, the development of Bi_2Te_3 thin-film materials with high ZT is urgent. Deposition methods, such as electrodeposition [11,12], sputtering [13–16], and evaporation [17,18], have been used to synthesize Bi_2Te_3 thin films. Nanostructures can be introduced into Bi_2Te_3 films to enhance their thermoelectric properties and reduce lattice thermal conductivity [18,19]. Tuning the carrier concentration n of Bi_2Te_3 films is another effective approach to enhance the ZT value because of the dependence of S, σ, and k_c on the

carrier concentration. Annealing can reduce the carrier concentration in n-type Bi_2Te_3 films, and an annealing temperature of 473 K was determined to be optimal for ZT improvement [14]. Introducing impurities into Bi_2Te_3-based compounds can also effectively adjust the carrier concentration. For example, Yang et al. studied the effects of Ag doping on the thermoelectric properties of n-type $Bi_2(Te_{0.94},Se_{0.06})_3$ [20]. The group found that at doping levels below 0.2 wt.%, Ag acted as an n-type donor; when the doping level exceeded 0.2 wt.%, the Ag atoms acted as p-type acceptors. Fan et al. investigated the effects of Bi doping on the thermoelectric performance of $Bi_xSb_{2-x}Te_3$ thin films and found that these films transformed from p-type semiconductors to n-type semiconductors as the Bi content increased [21]. Other impurities, such as Zn_4Sb_3, Se, SbI_3 and CuBr, were also investigated [22,23].

However, to the best of our knowledge, the effect of lead (Pb) doping on the thermoelectric properties of Bi_2Te_3 films has not been reported in the literature. Pb is a useful element for tuning the carrier concentration of Bi_2Te_3 bulk materials; moreover, doping of Pb atoms into the Bi_2Te_3 crystal lattice leads to an increase in hole concentration [24,25]. This work aims to tune the carrier concentration of n-type Bi_2Te_3 films through Pb doping and improve the thermoelectric properties of the Bi_2Te_3 film, because the high carrier concentration of typical n-type Bi_2Te_3 films limits the enhancement of ZT [13–16]. In this work, we adopted radiofrequency magnetron sputtering to synthesize Pb-doped n-type Bi_2Te_3 films, characterized the nanocrystalline structure of the films, and systematically investigated the effects of Pb doping on the thermoelectric properties of as-deposited and annealed Bi_2Te_3 films.

* Corresponding author. Tel.: +86 10 62797162; fax: +86 10 62771160.
  E-mail address: liliangliang@mail.tsinghua.edu.cn (L. Li).

2. Experimental

N-type Bi$_2$Te$_3$ films doped with Pb were deposited by radiofrequency magnetron sputtering on SiO$_2$ (300 nm)/Si substrates at room temperature (RT). A Bi$_2$Te$_3$ target (diameter, 3 in.; 99.999 at.%) and small pieces of Pb plates (size, 5 × 5 × 0.3 mm^3; 99.999 at.%) were used as source materials. Pb plates (0, 2, or 4 pieces) were fixed on the Bi$_2$Te$_3$ target by silver paste to adjust the doping concentration in the films. The base pressure in the sputtering chamber was below 1.5 × 10^{-4} Pa, the deposition pressure was 0.5 Pa, and the Ar gas flow was 10 sccm. Samples with two sizes (4 × 16 and 10 × 10 mm^2) were simultaneously deposited. The 4 × 16 mm^2 samples were used for the Seebeck measurement, and the 10 × 10 mm^2 samples were used for the Hall test and other investigations. The film thickness was ~300 nm for 1 h of sputtering.

The crystal structures and surface morphologies of the thin films were characterized by X-ray diffraction (XRD) with a D/max-RB diffractometer (Rigaku, Japan) using Cu Kα radiation and atomic force microscopy (AFM, Bruker Nanoscope IIIa MultiMode, Germany), respectively. The film compositions were determined by inductively coupled plasma-atomic emission spectrometry (ICP-AES, VISTA-MPX, Varian Inc., USA). σ, *n*, and mobility μ were measured using a Hall measurement setup (Resis-Hall test DC-8340, TOYO, Japan) from RT to 473 K under Ar protection.

The Seebeck coefficient was measured by a customized setup, which is shown schematically in Fig. 1. Two heaters with maximum power of 250 W were embedded in the base of a chamber. The voltages of the heaters were set differently using a voltage controller to ensure a temperature difference between the two ends of the sample. Meanwhile, the average temperature of the sample was continuously increased during heating. TT-T-36-SLE (*T*-type, Omega Engineering, Inc., USA) thermocouples with a measurement range of −73 K to 533 K were used to obtain the temperatures at the two ends. This type of thermocouple, which has a diameter of 0.127 mm, has an extremely short response time of less than 0.1 s and can accurately measure the dynamic temperature. The thermocouples were mechanically attached to the sample surface. The Cu wires of the two thermocouples were used to measure the Seebeck voltage (ΔV). A 34970A data acquisition unit equipped with a 34902A module (Agilent Technologies, Inc., USA) was used to record the sample temperatures (T_1 and T_2) and ΔV simultaneously T_1, T_2, and ΔV were recorded every 10 seconds. The electric contact was checked prior to the measurement. Sufficient electric contact was achieved when ΔV was within ±3 μV with the heaters turned off. Otherwise, the sample was reinstalled prior to the measurement.

The customized measurement setup was calibrated using a LaCo$_{0.85}$Cu$_{0.15}$O$_3$ sample whose Seebeck coefficient had been measured using ZEM-2 (Ulvac-Riko, Japan) [26]. Voltages of 70 and 60 V were applied to heaters 1 and 2, respectively (Fig. 1). The rising curves of T_1 and T_2 as a function of time *t* show dynamic characteristics (Fig. 2(a)). The temperature difference, $\Delta T = T_1 - T_2$, as a function of average temperature, $(T_1 + T_2)/2$, is given in Fig. 2(b). The ΔT varied between 4.3 and 10.3 K during the measurement, which was appropriate for the Seebeck coefficient measurement [27]. The intrinsic Seebeck coefficient of the sample was obtained by eliminating the Seebeck coefficient of the Cu wires from $\Delta V/\Delta T$ [28]. Table 1 summarizes the intrinsic Seebeck coefficients of the LaCo$_{0.85}$Cu$_{0.15}$O$_3$ sample measured by ZEM-2 and by the customized setup. The difference in the data obtained from the two setups is within 5.2%. Therefore, the Seebeck coefficient obtained by the customized setup is reliable.

3. Results and discussion

Table 2 summarizes the composition of the Pb-doped Bi$_2$Te$_3$ films synthesized by magnetron sputtering. When 0, 2, and 4 Pb plates were attached to the Bi$_2$Te$_3$ target, the corresponding 1#, 2#, and 3# samples had Pb concentrations of 0, 0.38, and 0.70 at.%, respectively. No Ag impurity was found in the samples.
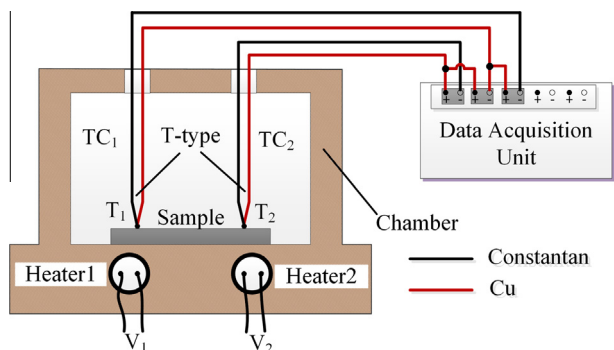

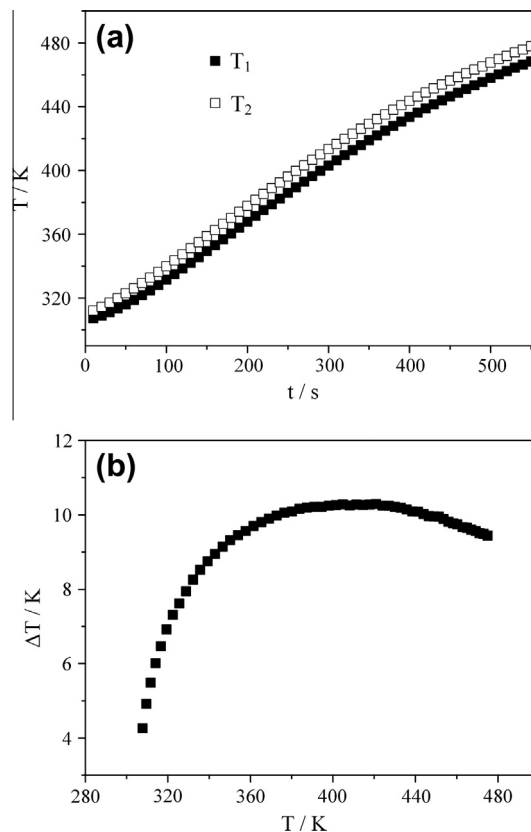**Fig. 1.** Schematic of the customized setup for the Seebeck coefficient measurements.

Fig. 2. Dynamic properties of the customized setup: (a) Temperature-increase curves at two ends of a LaCo$_{0.85}$Cu$_{0.15}$O$_3$ sample, and (b) temperature difference (ΔT) as a function of the average temperature of the sample.

The atomic ratio of Bi to Te is approximately 2:3. Fig. 3 shows the XRD patterns of the as-deposited and annealed films. All peaks related to the Bi–Te compound are indexed to the rhombohedral phase of Bi$_2$Te$_3$ (JCPDS No. 15-0863). After annealing, the intensities of the diffraction peaks of all three samples increase, and the full widths at half-maximum (FWHM) of the XRD peaks are slightly narrowed. These phenomena indicate the growth of grains. The grain sizes were calculated from the specimens' FWHM using Scherrer's equation [29]. The grain sizes of 1#, 2#, and 3# samples before annealing are 14.5, 14.5, and 12.6 nm, respectively. After annealing, the grain sizes of 1#, 2#, and 3# samples increase to 26.9, 22.5, and 21.9 nm, respectively. These values indicate that the films have nanocrystalline structures. The AFM images in Fig. 4 show the surface morphologies of the 1#, 2#, and 3# samples before and after annealing. A flaky surface was observed on the samples prior to annealing (Fig. 4(a–c)). The surface roughnesses of the 1# (Fig. 4(a)) and 3# (Fig. 4(c)) samples are higher than that of the 2# sample (Fig. 4(b)); thus, the surface morphologies of 1# and 3# are not very clear under AFM. After annealing, the crystal grains of all three samples became rounder, and nanocrystalline structures were clearly observed. The average grain sizes of the annealed samples are approximately 20–30 nm. These values are consistent with the grain sizes obtained from Scherrer's equation. A nanocrystalline structure contributes to the enhancement of the performance of thermoelectric materials because the structure promotes phonon scattering at the grain boundaries and causes an observable decrease in the lattice thermal conductivity [30,31].

Meanwhile, Hall test results indicate that the 1#, 2#, and 3# samples are all *n*-type semiconductors. The carrier concentrations of the as-deposited films from 300 K to 473 K are shown in Fig. 5(a). The *n* of sample 1# slightly varies with the temperature,